

Iron(III)–salen–H₂O₂ as a peroxidase model: electron transfer reactions with anilines

Adhem Mohamed Aslam · Seenivasan Rajagopal ·
Mariappanadar Vairamani · Maddula Ravikumar

Received: 6 June 2011 / Accepted: 8 August 2011 / Published online: 7 September 2011
© Springer Science+Business Media B.V. 2011

Abstract Iron(III)–salen complexes catalyze the H₂O₂ oxidation of various ring-substituted anilines in MeCN have been studied, and [O=Fe^{IV}(salen)]⁺ is proposed as the active species. Study of the kinetics of the reaction by spectrophotometry shows the emergence of a new peak at 445 nm in the spectrum which corresponds to azobenzene. Further oxidation of azobenzene by H₂O₂ leads to the formation of azoxybenzene. ESI–MS studies also support the formation of these products. The rate constants for the oxidation of *meta*- and *para*-substituted anilines were determined from the rate of decay of oxidant as well as the rate of formation of azobenzene, and the reaction follows Michaelis–Menten kinetics. The rate data show a linear relationship with the Hammett σ constants and yield a ρ value of -1.1 to -2.4 for substituent variation in the anilines. A reaction mechanism involving electron transfer from aniline to [O=Fe(salen)]⁺ is proposed. The presence of axial ligands modulates the activity of the complex.

Introduction

Iron plays an important role in biological systems, as enzymes containing Fe(II) and Fe(III) are of crucial importance in electron transfer reactions and in the activation and transport of small molecules such as molecular oxygen [1, 2]. Most mononuclear non-heme iron enzymes contain iron ligated by oxygen and/or nitrogen donor ligands [3, 4]. Many of these enzymes promote dioxygen activation, resulting in the formation of highly reactive iron-peroxo (Fe^{III}–OOH, Fe^{III}–O₂[−]) or iron-oxo (Fe^{IV}=O or Fe^V=O) species as oxidants. The porphyrin iron(III)–hydroperoxo complex, (Por)Fe(III)–OOH or compound **0**, was detected for horseradish peroxidase [5, 6], at low temperature in the presence of high concentrations of hydrogen peroxide. The transient formation of porphyrin iron hydroperoxo species was also detected for the Arg38LeuHRP mutant [7]. Compound **0** and its deprotonated form (Por)Fe^(III)–OO[−] are species encountered in P450 chemistry and precede an isoelectronic analogue of peroxidases, compound **I** [Por^{•+}Fe^{IV}=O] in the reaction cycle [8]. Our understanding of the formation of high valent iron oxo or iron peroxo intermediates for peroxidases and cytochrome P450 chemistry has benefited from the use of synthetic metalloporphyrin models [1–4, 9–12]. Oxoiron(IV) species are typically invoked as the reactive intermediates both in heme and in non-heme iron-dependent oxygenases [13–16]. While the existence of high valent oxoiron species has been well established for some time in the chemistry of heme enzymes [17], as well as in iron-porphyrin model compounds [18], only more recently have the corresponding non-heme iron examples been identified [13, 14, 19–24].

In recent years, metal-salen [salen = 1,6-bis(2-hydroxyphenyl)-2,5 diazahexa-1,5 diene] complexes have been

Electronic supplementary material The online version of this article (doi:10.1007/s11243-011-9529-4) contains supplementary material, which is available to authorized users.

A. M. Aslam (✉)
Department of Chemistry, M. S. S. Wakf Board College,
Madurai 625 020, India
e-mail: adamaslam19@gmail.com

S. Rajagopal
School of Chemistry, Madurai Kamaraj University,
Madurai 625 021, India

M. Vairamani · M. Ravikumar
National Centre for Mass Spectrometry, Indian Institute
of Chemical Technology, Hyderabad 500 007, India

extensively used for the oxidation of a variety of organic substrates, epoxidations [25–29], sulfoxidations [30–39], ring opening reactions [40–45], fixation of CO₂, etc. [46, 47]. The iron salen complexes may be considered as models of non-heme iron enzymes bearing tyrosine residues, which also play an important and diverse role in catalysis [48]. A coordinated tyrosine residue is found for mononuclear non-heme iron(III) enzymes such as protocatechuate 3,4-dioxygenase (3,4-PCD) bearing the His₂Tyr₂ coordination environment [49, 50]. A salen ligand well reproduces the coordination environment of two His and two Tyr units.

We have recently reported on the generation of oxoiron species from the reaction of iron(III)–salen complex with PhIO [51, 52]. The oxoiron species was characterized by spectroscopic techniques and was formulated as [O=Fe(salen)]⁺. From an NMR study, Bryliakov and Talsi [34, 35] have proposed the active reactive species as an iron(III)–salen–PhIO adduct at low temperature. However, our recent Mossbauer study indicates that the active species involves iron in the iron(IV) oxidation state [51, 52]. These oxo(salen)iron complexes selectively oxidize organic sulfides to sulfoxides. The reactions follow Michaelis–Menten type kinetics, and oxygen atom transfer from the oxidant to substrate has been proposed as the mechanism of the reaction.

From the green chemistry and biochemistry point of view, it is better to use environmentally benign H₂O₂ as an oxidant to generate oxoiron intermediates. Hence, we have investigated the reaction of iron(III)–salen complex with H₂O₂ to generate a reactive oxoiron species. This reactive species undergoes interesting reactions with anilines to form azobenzene and azoxybenzene as the major products.

In this report, we present spectroscopic, kinetic and mechanistic data for the iron(III)–salen catalyzed H₂O₂ oxidation of *meta*-, *ortho*- and *para*-substituted anilines. Based on our results, we propose an electron transfer mechanism for the reaction.

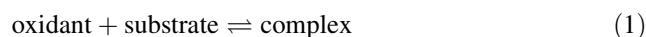
Results

Seven iron(III)–salen complexes (1–7, Chart 1) have been synthesized and characterized as detailed in the Experimental section and as shown in Table 1. The reactions of these iron(III)–salen complexes with H₂O₂ were examined by UV–Vis spectrophotometry using a diode array spectrophotometer. Figure 1 shows the changes during the reaction of 1 with H₂O₂ in the absence of substrate. The iron(III)–salen complex has an absorption maximum at 470 nm, and upon the addition of 25-fold excess of H₂O₂, there is a decrease in this absorbance with concomitant increases at 365 nm and in the broad 550–800 nm region. These changes

indicate the formation of a (salen) Fe^{III}–OOH species. As illustrated in Fig. 2, the decay of absorbance at 470 nm is accompanied by the growth of a feature assigned to compound 1, at 680 nm. These features are similar to those observed for iron(IV) oxoporphyrin cation radicals [53]. The observed spectroscopic changes can therefore be assigned to heterolytic scission of the O–O bond to furnish the species A ([O=Fe(salen)]⁺) as the active oxidant.

Kinetics

Figure 3 shows the change in absorbance of oxidant generated from 5 and H₂O₂ with time in the presence of aniline. The decay exhibited a typical single exponential behavior and was strongly dependent on substrate concentration. Saturation behavior was observed at higher concentrations of substrate (Fig. 4), supporting the notion that the substrate binds to the oxidant before the rate controlling step. Thus, the reaction proceeds through Michaelis–Menten type kinetics (Eqs. 1, 2)



On the basis of the Michaelis–Menten formulation, the observed rate constant is given by Eq. 3. The details of derivation of the rate constant data from the change in absorbance with time are given in the Experimental section. The rearrangement of Eq. 3 leads to Eq. 4.

$$k_1 = k_{\text{obs}} = k [\text{substrate}] / (K_M + [\text{substrate}]) \quad (3)$$

$$1/k_1 = 1/k + K_M/k [\text{substrate}] \quad (4)$$

where K_M is the Michaelis–Menten constant and k is the rate constant for the decay of the active oxidant. From the plot of $1/k_1$ versus $1/[\text{substrate}]$, the values of k and K_M were evaluated and are collected in Table 2. The reaction of complex 6 with anilines in the presence of H₂O₂ was analyzed in the same way, and the kinetic data are also given in Table 2. When the concentration of substrate is increased, apart from the decay of oxidant, we are also able to see the growth of a peak at 445 nm corresponding to the formation of azobenzene (See ESI, Figure S1).

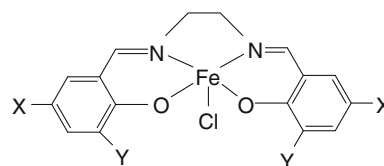
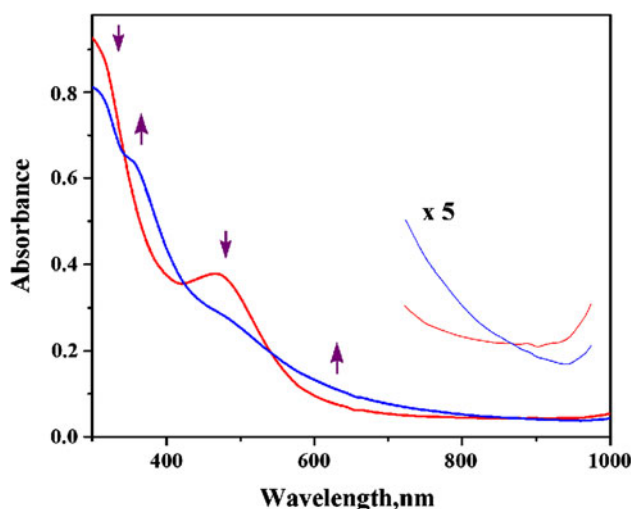


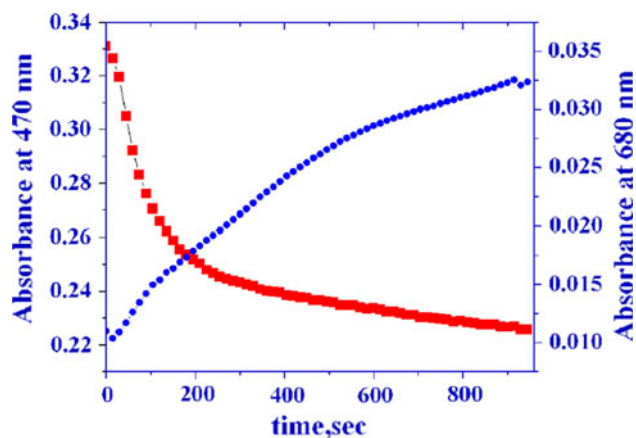
Chart 1 Structure of iron(III)–salen complexes. 1, X = Y = H; 2, X = Cl, Y = H; 3, X = Br, Y = H; 4, X = Me, Y = H; 5, X = OMe, Y = H; 6, X = Y = *t*-Bu; 7, X = Y = Cl

Table 1 Spectral data and $E_{1/2}$ (V) values for iron(III)–salen complexes

Complexes	λ_{\max} (MeCN)/nm, ($\ell/\text{dm}^3 \text{ mol}^{-1} \text{ cm}^{-1}$)	ESI–MS data	IR data, cm^{-1}		$E_{1/2}$ (V) versus (SCE)
			$\nu_{\text{C=N}}$	$\nu_{\text{C-O}}$	
1	301, 470 (9,038, 4,088)	322	1,628	1,294	–0.28
2	358, 472 (16,905, 3,955)	391	1,635	1,252	–0.24
3	242, 467 (34,000, 6,509)	478	1,637	1,293	–0.25
4	301, 489 (12,275, 4,816)	350	1,621	1,301	–0.41
5	304, 501 (15,250, 5,515)	382	1,624	1,300	–0.44
6	322, 503 (11,863, 5,796)	546	1,614	1,304	–0.68
7	308, 477 (32,250, 5,379)	460	1,637	1,213	–0.20

**Fig. 1** UV–Vis spectrum of **1** in the absence H_2O_2 (red line); in the presence of H_2O_2 (blue line) in MeCN at 25 °C. $[\text{H}_2\text{O}_2] = 2 \times 10^{-3} \text{ M}$; $[\mathbf{1}] = 8 \times 10^{-5} \text{ M}$

With the other iron(III)–salen complexes, **1–4** and **7**, the reaction is faster and we were not able to follow the decrease in absorbance of the reactive oxidant generated from iron(III)–salen and H_2O_2 using a diode array spectrophotometer. Immediately after adding H_2O_2 to a mixture of iron(III)–salen and aniline, the peak corresponding to the active oxidizing species disappeared and a peak corresponding to the product appeared at 445 nm. Hence for all the other iron(III)–salen complexes **1–4** and **7** and also for **5** and **6**, the progress of the reaction was monitored at 445 nm where azobenzene shows strong absorption. The changes in the absorbance of **1**– H_2O_2 mixture in the presence of aniline with time are shown in the supplementary information (See

**Fig. 2** Change in absorbance with time for the disappearance of iron(III)–salen complex at 470 nm (red points) and concomitant appearance of oxointermediate (compound A) at 680 nm (blue points)

ESI, Figure S2). When other anilines were used as substrates, similar spectroscopic changes were observed, and the changes in the reaction of oxidant with *para*-anisidine are shown in the supplementary information (See ESI, Figure S3). Apart from the peak at 450 nm which corresponds to azobenzene, there is increase in absorbance at 325 nm due to the formation of azoxybenzene. The pseudo first-order rate constants were obtained from the plot of $\log \text{OD}$ versus time, which was linear for the initial part. Here again, Michaelis–Menten type behavior was observed.

To quantify the substituent effect for the oxidation of anilines with H_2O_2 in the presence of **5** and **6**, the $\log k$ values of *meta*- and *para*-substituted anilines were plotted against Hammett σ as well as Brown–Okamoto σ^+ constants. The experimental data correlated better with σ constants than σ^+ ,

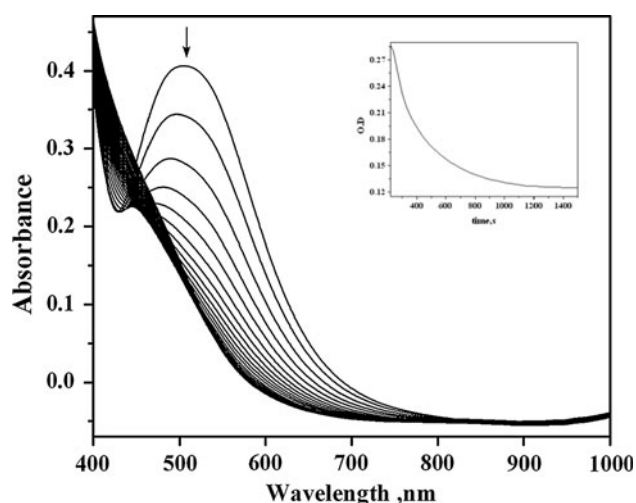


Fig. 3 Change in absorbance of **5** with time in the presence of H_2O_2 and aniline. $[\mathbf{5}] = 8 \times 10^{-5} \text{ M}$, $[\text{H}_2\text{O}_2] = 2 \times 10^{-3} \text{ M}$, $[\text{aniline}] = 4 \times 10^{-3} \text{ M}$. Inset change in absorbance of **5** with time at 510 nm

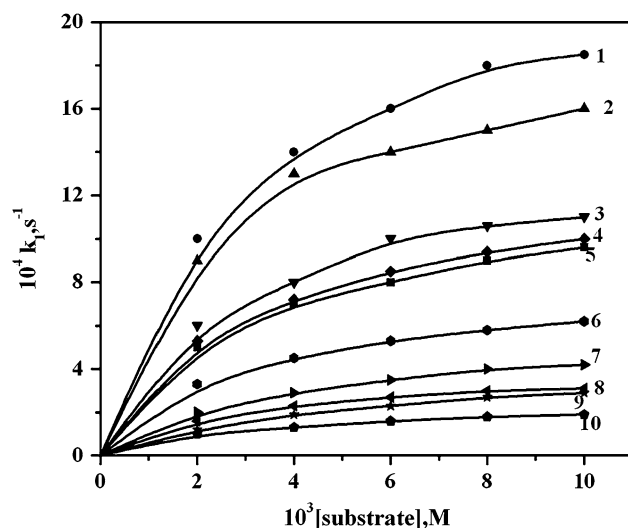


Fig. 4 Plot of k_1 versus $[\text{substrate}]$ for the oxidation of ring-substituted anilines with **5** at 298 K (the points 1–10 are referred by the same numbers as given in Table 2)

and a sample plot is shown in Fig. 5. The reaction constant value (ρ) is negative, and its magnitude depends on the nature of substituent in the salen ligand. The ρ value was -1.2 ($r = 0.99$) for **5** and -2.5 ($r = 0.97$) for **6**. The negative ρ values indicate that a positive charge is developed on the nitrogen center of the substrate in the transition state of the reaction.

The rate constants (k') for the formation of azobenzene were calculated from the double reciprocal plots of k_1 versus $[\text{substrate}]$ for 11 ring-substituted anilines, and the data are presented in Table 3. The Michaelis–Menten constants are given in the ESI, Table S1. To quantify the substituent effect on the rate of formation of product, the log

Table 2 Rate constant (k) and Michaelis–Menten constant (K_M) values for iron(III)–salen– H_2O_2 system oxidation of $\text{XC}_6\text{H}_4\text{NH}_2$ in MeCN at 298 K (determined from the decay of the oxidant)

S. no.	X	$10^3 k \text{ M}^{-1} \text{ s}^{-1}$		$10^3 K_M$	
		5	6	5	6
1	2-OCH₃	24.0 ± 0.06	–	2.9	–
2	4-CH₃	18.0 ± 0.02	62.5 ± 0.10	3.0	3.5
3	3-CH₃	14.3 ± 0.03	21.8 ± 0.03	3.0	3.8
4	2-CH₃	12.7 ± 0.02	16.6 ± 0.03	2.9	2.8
5	H	12.4 ± 0.03	10.1 ± 0.02	3.0	3.0
6	3-OCH₃	7.8 ± 0.02	6.2 ± 0.01	2.9	2.8
7	4-Cl	6.1 ± 0.02	2.4 ± 0.01	2.7	3.8
8	4-Br	5.5 ± 0.01	2.3 ± 0.01	2.8	2.7
9	3-Cl	3.9 ± 0.01	1.7 ± 0.01	2.8	2.9
10	4-NO₂	1.6 ± 0.01	0.2 ± 0.01	2.8	2.4
ρ		-1.2	-2.5		
r		0.99	0.97		

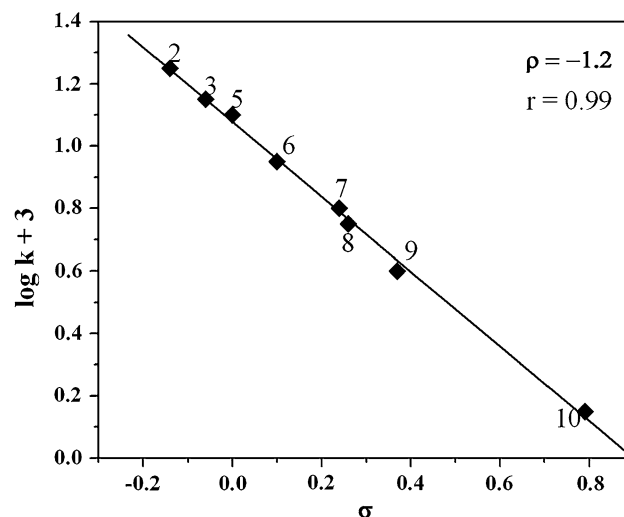


Fig. 5 Hammett plot for the oxidation of $\text{X-C}_6\text{H}_4\text{NH}_2$ with **5** at 298 K

k' values of *meta*- and *para*-substituted anilines were plotted against Hammett σ and Brown–Okamoto σ^+ constants. Since the formation of azobenzene involves the reaction of anilinium cation radical, which may be stabilized through resonance interaction with electron-releasing substituents in the *ortho*- or *para*-positions, the experimental data are better correlated with σ^+ constants rather than σ constants. The ρ^+ value for **1** is -1.5 ($r = 0.99$) and ρ value is -2.0 ($r = 0.96$). The reaction constant value is negative, and its magnitude depends on the nature of substituent in the salen ligand. The ρ^+ value was found to vary between -1.4 and -2.3 . The negative ρ^+ values indicate that a positive charge is developed on the nitrogen center of the substrate at the

Table 3 Rate constant (k') values for iron(III)–salen–H₂O₂ system oxidation of XC₆H₄–NH₂ in MeCN at 298 K (determined from the formation of product)

S. no.	X	10 ⁴ k M ⁻¹ s ⁻¹							ρ^+	r
		1	2	3	4	5	6	7		
1	4-CH ₃	200 ± 3.4	411 ± 10.3	290 ± 6.4	40.3 ± 1.2	19.8 ± 0.4	83.6 ± 2.2	468 ± 11.2	0.9	0.99
2	2-CH ₃	87.7 ± 2.2	133 ± 2.4	94.5 ± 2.6	14.5 ± 0.35	9.9 ± 0.21	16.7 ± 0.42	51.6 ± 1.34	0.4	0.98
3	4-CH ₃	37.8 ± 0.52	68.5 ± 1.4	51.2 ± 0.77	15.9 ± 0.3	4.00 ± 0.07	14.8 ± 0.29	82.0 ± 2.0	0.6	0.99
4	3-CH ₃	20.4 ± 0.40	38.8 ± 0.78	29.4 ± 0.62	7.00 ± 0.2	3.80 ± 0.1	1.00 ± 0.02	34.3 ± 0.62	0.5	0.97
5	2-CH ₃	20.5 ± 0.48	31.9 ± 0.54	30.0 ± 0.54	3.90 ± 0.06	3.30 ± 0.06	1.2 ± 0.02	35.1 ± 0.8	0.6	0.96
6	H	18.1 ± 0.54	29.2 ± 0.6	21.2 ± 0.5	5.30 ± 0.16	1.60 ± 0.05	1.90 ± 0.06	55.5 ± 2.0	0.7	0.99
7	3-OCH ₃	11.9 ± 0.26	18.2 ± 0.4	18.1 ± 0.5	1.70 ± 0.05	0.82 ± 0.04	0.70 ± 0.03	18.2 ± 0.7	0.8	0.96
8	4-Cl	7.30 ± 0.10	10.8 ± 0.3	9.70 ± 0.27	2.40 ± 0.07	0.80 ± 0.03	0.87 ± 0.04	20.1 ± 0.9	0.6	0.99
9	4-Br	6.70 ± 0.09	9.60 ± 0.2	9.20 ± 0.5	2.40 ± 0.1	0.60 ± 0.03	0.71 ± 0.03	13.7 ± 0.6	0.7	0.99
10	3-Cl	3.80 ± 0.12	7.00 ± 0.4	4.70 ± 0.2	1.20 ± 0.05	0.44 ± 0.02	0.60 ± 0.03	4.68 ± 0.3	0.6	0.98
11	4-NO ₂	0.82 ± 0.03	1.10 ± 0.03	1.00 ± 0.05	0.37 ± 0.02	–	–	1.28 ± 0.06	0.5	0.99
ρ^+		–1.5	–1.6	–1.6	–1.4	–1.4	–2.3	–1.7	–	–
r		0.99	0.99	0.99	0.97	0.97	0.96	0.98	–	–

transition state of the reaction. The effects of substituents on the salen ligand were also studied. Here also a plot of $\log k'$ versus σ^+ was linear, giving positive ρ^+ values in the range of 0.4–0.9 (Table 3). The positive ρ^+ values indicate that negative charge is developed at the metal center in the transition state. It is interesting to recall that we previously obtained ρ values in the range of 1.4–2.3 for a series of [oxo(salen)chromium(V)]⁺ ions in the oxidation of ring-substituted anilines [54].

ESI–MS and ¹H NMR studies

We undertook a systematic study of the products formed in these aniline oxidation reactions using ESI–MS technique.

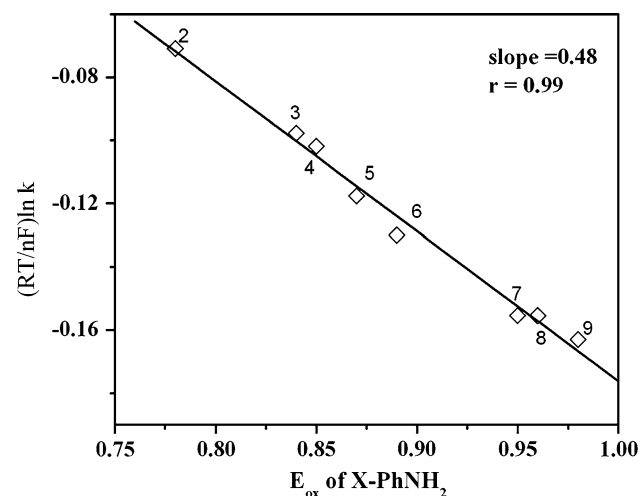
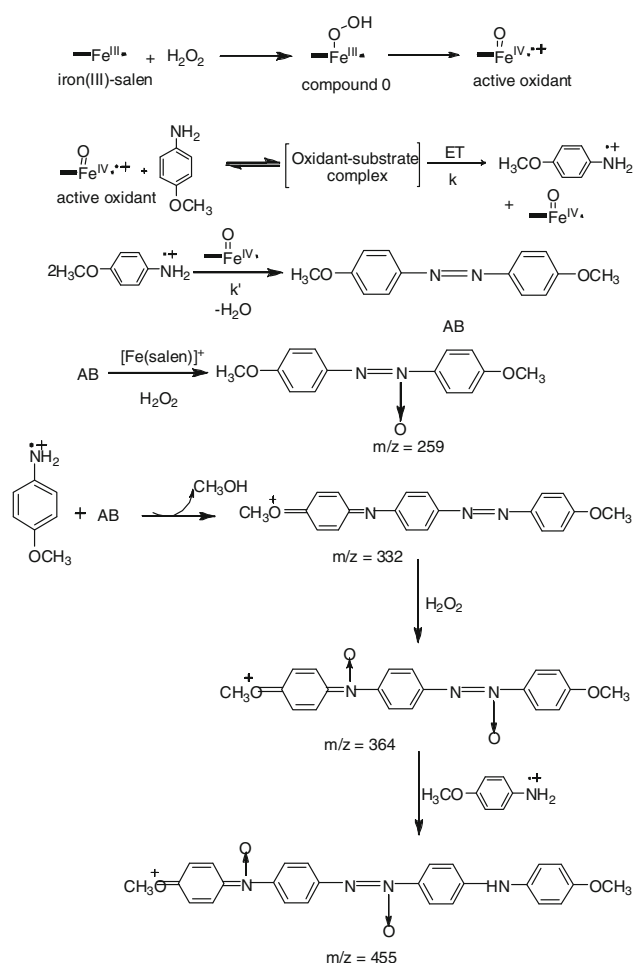


Fig. 6 Plot of oxidation potential of anilines versus $(RT/nF) \ln k$ (the points 2–9 are referred by the same numbers as given in Table 2)

The ESI–MS spectra of the reaction mixtures prepared using aniline as substrate and the iron(III)–salen–H₂O₂ system as oxidant were recorded by direct infusion of the reaction mixture at definite intervals of time (1, 10, 30, 60 min). The intensity of the peak with m/z value 199 increased with time (See ESI, Figure S4). This peak corresponds to azoxybenzene. Further corroboration of this assignment was obtained by observing the expected shifts in m/z values when we used *meta*- and *para*-substituted anilines instead of the parent aniline. Thus, when *para*-anisidine was used as the substrate, a peak with m/z value 259 was formed (a shift of 60 Da), confirming the formation of *para*-azoxy anisole. The ESI–MS data also reveal the formation of peaks with m/z values 332, 364 and 455, corresponding to N-oxygenated oligomers which are formed by condensation of oxidized products and radicals formed in the reaction (Scheme 1). The use of 4-bromo-aniline as substrate with its characteristic 1:1 ⁷⁹Br:⁸¹Br isotope distribution afforded a characteristic pattern of peaks spaced at intervals of two mass units at m/z 355, 357, 359 (See ESI, Figure S5) which allowed us to unambiguously assign the nature of product formed. It is interesting to mention here that our previous study of oxidation of anilines using [oxo(salen)chromium(V)]⁺ ions resulted in the formation of emeraldine type oligomers of aniline [54].

A ¹H NMR sample spectrum of one of the products of these reactions is shown in ESI, Figure S6. The number of signals observed for the product is consistent with the proposed formation of azobenzene. Two sets of resonances can be readily identified by ¹H NMR. The shift pattern for the protons of the aromatic rings further substantiates the formation of azobenzene, with four protons giving a signal at δ 7.9 and six protons giving a signal at δ 7.5.



Scheme 1 Mechanism of iron(III)-salen catalyzed H_2O_2 oxidation of anilines

Effect of axial ligands on the oxidation of anilines

The catalytic activity of metal-salen ions in oxidation reactions can be tuned not only by making substitutions in the salen ligand, but also by adding donor ligands to the reaction mixture [36–38, 55–57]. The added ligands bind to the axial position of the metal-salen complex and mimic the effects of the axial histidine and thiolate residues found in peroxidases and cytochrome P-450s, respectively [58]. For better understanding the role of axial ligands in activating these iron(III)-salen catalyst, we added imidazole (Im) or N-methylimidazole (NmIm) to the iron(III)-salen complexes and recorded the ESI-MS spectra. The spectra show that a molecule of the donor ligand is coordinated to the metal center at the axial coordination site. For example when Im was added, the parent iron(III)-salen ion ($m/z = 322$) disappeared and a new peak with m/z value 390 was observed which corresponds to the iron(III)-salen-Im adduct (see ESI, Figure S7). In the UV-Vis spectrum, the addition of imidazole shifted the λ_{max} value of the

Table 4 Rate constants (k') values for iron(III)-salen- H_2O_2 system oxidation of $\text{X-C}_6\text{H}_4\text{-NH}_2$ in MeCN at 298 K in the absence and presence of added ligands(AL)

Substrate	Absence of AL	Im	NmIm
4-OCH₃	200 ± 3.4	412 ± 8.1	764 ± 16.8
2-OCH₃	87.7 ± 2.2	132 ± 2.7	233 ± 4.2
4-CH₃	37.8 ± 0.52	69.4 ± 1.3	138 ± 3.1
3-CH₃	20.4 ± 0.40	42.7 ± 0.48	78.0 ± 1.6
2-CH₃	20.5 ± 0.48	37.1 ± 0.60	77.0 ± 1.9
H	18.1 ± 0.54	32.5 ± 0.45	68.5 ± 2.1
3-OCH₃	11.9 ± 0.26	24.7 ± 0.42	51.8 ± 1.3
4-Cl	7.30 ± 0.10	14.1 ± 0.31	27.5 ± 0.5
4-Br	6.70 ± 0.09	12.4 ± 0.17	23.6 ± 0.42
3-Cl	3.80 ± 0.12	6.5 ± 0.11	13.1 ± 0.15
4-NO₂	0.82 ± 0.03	1.2 ± 0.08	2.7 ± 0.09
ρ^+	-1.5	-1.6	-1.6
r	0.99	0.99	0.98

iron(III)-salen ion substantially (see ESI, Figure S8), from 467 to 504 nm in the case of iron(III)-salen **1** and from 501 to 560 nm for complex **5**.

The rate of the title reaction is accelerated in the presence of imidazole and N-methyl imidazole, whereas these bases completely inhibited the rate of sulfoxidation in the iron(III)-salen-PhIO redox system [51, 52]. The kinetic data observed in the presence of Im and NmIm for the title reaction are collected in Table 4. The rate of iron(III)-salen catalyzed H_2O_2 oxidation of aniline in the presence of imidazole is also sensitive to the aryl substituent of aniline (Table 4). Application of the Brown-Okamoto equation to these kinetic data was successful, and the reaction constant (ρ^+) values are given in Table 4.

Discussion

The results presented above clearly indicate that the iron(III)-salen- H_2O_2 system is capable of transforming a range of substituted anilines to the corresponding azo and azoxy derivatives. The kinetic data point to Michaelis-Menten type behavior, and the reaction is first order in the oxidant and fractional order with respect to anilines. UV-Visible spectroscopic studies reveal that at early stage of the reaction, the only significant product is azobenzene, shown by the increase in absorbance at 445 nm, but this is slowly converted to azoxybenzene and higher oligomers by further reaction with H_2O_2 . When H_2O_2 is added last, it reacts with the complex to produce $[\text{Fe}^{\text{IV}}=\text{O}(\text{salen})]^+$ which initiates the reaction. Electron transfer from aniline to the active oxidant $[\text{Fe}^{\text{IV}}=\text{O}(\text{salen})]^+$ results in the formation of anilinium radical ions, which couple to produce

azobenzene. Further reaction between azoxybenzene and anilinium radicals results in the formation of N-oxygenated trimers and tetramers. The ESI–MS study of the oxidation of 4-methoxyaniline gives peaks with m/z values 332 and 455 (see ESI, Figure S9), corresponding to the trimer and tetramer of 4-methoxyaniline, respectively. Similar results were observed by Li et al. [59] for the Mn(III)/(IV) oxidation of 4-methoxyaniline.

We propose that the reaction between the active oxidant generated from the iron(III)–salen–H₂O₂ system and anilines is initiated through electron transfer (ET) from the substrate to the oxidant. Additional support for the proposal of ET at the rate controlling step is provided from the plot of RT/F (ln k) versus oxidation potential of the anilines (slope = 0.47, $r = 0.98$, Fig. 6). The linearity of the plot and the slope close to 0.5 are in favor of an ET transfer mechanism [60, 61]. On the basis of these observations, we propose the mechanism shown in Scheme 1 for the oxidation of anilines with iron(III)–salen–H₂O₂ to account for this reaction.

The catalytic effect of imidazoles on this system deserves explanation. In many peroxidases, the catalytically active iron center is coordinated by the four pyrrole nitrogen atoms of its heme ligand plus an axial imidazole [62], which is believed to facilitate O–O heterolysis. Imidazole and its derivatives have been found to have catalytic effects in manganese catalyzed epoxidation reactions, especially with H₂O₂ as the source of oxygen [63–65]. We have observed large catalytic effects of ligand oxides on the sulfoxidation of organic sulfides with [oxo(salen)chromium(V)]⁺ ions [36–38]. This catalytic effect has been attributed to the strong binding of ligand oxides to the metal center, thereby weakening the M=O bond and facilitating oxygen atom transfer to the substrate. On the other hand, a different explanation has been provided for the catalytic role of imidazole in the epoxidations with [hydroperoxo–Mn(salen)] species. In the presence of imidazole, [hydroperoxo–Mn(salen)] species is converted into a [O=Mn(salen)]⁺ ion which is a more powerful oxidant than the former species. We propose that the conversion of (salen)Fe(III)–OOH into a higher oxidation state oxoiron species is facilitated in the presence of imidazoles. Thus, imidazole facilitates the heterolytic scission of (salen)Fe(III)–OOH to produce oxoiron species. This proposal is supported by the substantial red shift in the λ_{\max} of iron(III)–salen ions in the presence of imidazoles and by the ESI–MS studies.

Experimental

Salen ligands were prepared from ethylene diamine and the corresponding salicylaldehydes (Aldrich) by standard

methods [30–39, 51, 52]. The iron(III)–salen complexes 1–7 were prepared by the reaction of stoichiometric amounts of the ligands with iron(III)–chloride in EtOH and recrystallized from appropriate solvents [66–69]. The complexes (Chart 1) were characterized by UV–Vis, IR and ESI–MS techniques (Table 1).

Substituted anilines (Aldrich and Fluka) were purified by distillation under reduced pressure or recrystallization as already reported [70]. Reaction solutions were prepared in MeCN, kept under nitrogen and stored in bottles fitted with Teflon stoppers.

Kinetic measurements

An Analytic-Jena Specord S100 diode array spectrophotometer was used to record the absorption spectra of the complexes and to follow the kinetics of the reaction. The active oxidizing species was generated by mixing the complex with H₂O₂ in the ratio of 1:25. Reaction mixtures were prepared with H₂O₂ added last to prevent the accumulation of oxidant before the reaction. The kinetics of oxidation of a series of ring-substituted anilines were followed under pseudo first-order conditions in the presence of at least a 25-fold excess of substrate over the oxidant by measuring the decay in absorbance of the oxidizing intermediate. Since the reaction is fast, the rate measurements were difficult using a diode array spectrophotometer. However, we were able to follow the decay of the oxidizing intermediates generated from 5,5'-dimethoxy salen–iron(III) complex and 3,3',5,5'-tetra-*tert*-butyl salen–iron(III) at 510 and 503 nm, respectively.

Electrospray ionization mass spectra were acquired using a Quattro LC mass spectrometer (micro-mass, Manchester, UK) using the Masslynx data system. Samples were introduced into the source by a direct infusion pump (Harvard apparatus) at a rate of 5 μ L/min. Capillary and cone voltages were 4 and 20 kV, respectively. The progress of the reaction was followed at different time intervals to identify the intermediates and products.

Product analysis

In a typical experiment, 0.4 mM of substrate was added to a solution containing 0.4 mM of the complex and 0.4 mM of H₂O₂ in 5 ml of MeCN. The solution was stirred at 298 K for 1–12 h depending upon the nature of the aniline and complex. After the removal of the solvent under reduced pressure, the organic product was extracted with dichloromethane. The extract was dried and the solvent removed. The product mixture was analyzed by GC–MS using an Agilent 6890 GC (Agilent Technologies, USA)

equipped with a model 5,973 N mass selective detector, and also by ^1H NMR spectroscopy in CDCl_3 (See ESI, Figure S6).

Conclusion

Iron(III)–salen complexes efficiently catalyze the H_2O_2 oxidation of ring-substituted anilines to azobenzenes which are transformed to azoxybenzenes and oligomers of anilines in the presence of excess H_2O_2 . A mechanism involving ET from aniline to the active intermediate $[\text{O}=\text{Fe}^{\text{IV}}(\text{salen})]^+$ is proposed as the rate-controlling step. The presence of axial donor co-ligands, Im and NmIm speeds up the reaction.

Acknowledgments S. R. thanks DST for providing financial assistance in the form of project and UGC for sanctioning the DRS project for the School of Chemistry from which the instruments used for the study were procured. A. M. A. thanks UGC, the Principal and the Management, M. S. S. Wakf Board College, Madurai, for sanctioning leave under the FIP program.

References

- Ortiz De Montellano PR (ed) (2005) Cytochrome P-450 structure, mechanism and biochemistry, 3rd edn. Plenum press, New York
- Fujji H (2002) *Coord Chem Rev* 226:51
- Que L Jr, Ho RYN (1996) *Chem Rev* 96:2607
- Que L Jr (2000) *Nat Struct Biol* 7:182
- Back HK, Van Wart HE (1989) *Biochemistry* 28:5714
- Back HK, Van Wart HE (1992) *J Am Chem Soc* 114:718
- Rodriguez-Lopez JN, Smith AT, Thomley RNF (1996) *J Biol Chem* 271:4023
- Coon MJ, Vaz ADN, Mcginnity DF, Peng HM (1998) *Drug Metab Dispos* 26:1190
- Groves JT, Watanabe Y (1988) *J Am Chem Soc* 110:8443
- Bell SEJ, Cooke PR, Inchely P, Leonard DR, Lindsay Smith JR, Robbins A (1991) *J Chem Soc Perkin Trans* 2:549
- Meunier B (1992) *Chem Rev* 92:1411
- Groves JT, Gross Z, Stern MK (1994) *Inorg Chem* 33:5065
- Costas M, Mehn MP, Jensen MP, Que L Jr (2004) *Chem Rev* 104:939
- Price JC, Barr EW, Glass TE, Krebs C, Bollinger JM (2003) *J Am Chem Soc* 125:13008
- Abu-Omar MM, Loaiza A, Hontzas N (2005) *Chem Rev* 105:2227
- Newscomb M, Zhang R, Chandrasena REP, Halgrimson JA, Horner JH, Makris TM, Sligar SG (2006) *J Am Chem Soc* 128:4580
- Schlichting I, Berndzen J, Chu K, Stock AM, Maves SA, Benson DE, Sweet RM, Ringe D, Petsko A, Sligar SG (2000) *Science* 287:1615
- Groves JT, Han YZ (1995) Models and mechanism of cytochrome p450 action. In: Ortiz de Montellano PR (ed) *Cytochrome P450. Structure, mechanism and biochemistry*, 2nd edn. Plenum press, New York, pp 3–48
- Wallar BJ, Lipscomb JD (1996) *Chem Rev* 96:2625
- Tshuva EY, Lippard SJ (2004) *Chem Rev* 104:987
- Kryatov SV, Rybak-Akimova EV, Schindler S (2005) *Chem Rev* 105:2175
- Kim SO, Sastri CV, Seo MS, Kim J, Nam W (2005) *J Am Chem Soc* 127:4178
- Oh NY, Suh Y, Park MJ, Seo MS, Kim J, Nam W (2005) *Angew Chem Int Ed* 44:4235
- Berry JF, Bill E, Bothi E, Neese F, Wieghardt K (2006) *J Am Chem Soc* 128:13515
- Canali L, Sherrington DC (1999) *Chem Soc Rev* 28:85
- Katsuki T (1995) *Coord Chem Rev* 140:189
- Ito YN, Katsuki T (1999) *Bull Chem Soc Jpn* 72:603
- Jacobsen EN (1995) In: Wilkinson G, Stone FGA, Abel EW, Hegedus LS, (eds) *Comprehensive organometallic chemistry II*, vol 12, chap II. Pergamon, New York
- McGarrigle EM, Gilheany DG (2005) *Chem Rev* 105:1563
- Chellamani A, Alhaji NMI, Rajagopal S, Sevel R, Srinivasan C (1995) *Tetrahedron* 51:12677
- Chellamani A, Alhaji NMI, Rajagopal S (1997) *J Chem Soc Perkin Trans* 2:299
- Chellamani A, Kulandaipandi P, Rajagopal S (1999) *J Org Chem* 64:2232
- Sevel R, Rajagopal S, Srinivasan C, Alhaji NMI, Chellamani A (2000) *J Org Chem* 65:3334
- Bryliakov KP, Talsi EP (2004) *Angew Chem Int Ed* 43:5228
- Bryliakov KP, Talsi EP (2007) *Chem Eur J* 13:8045
- Venkataramanan NS, Premsingh S, Rajagopal S, Pitchumani K (2003) *J Org Chem* 68:1506
- Venkataramanan NS, Rajagopal S (2006) *Tetrahedron* 62:5645
- Venkataramanan NS, Rajagopal S, Vairamani M (2007) *J Inorg Biochem* 101:274
- Venkataramanan NS, Kuppuraj G, Rajagopal S (2005) *Coord Chem Rev* 249:1249
- Jacobsen EN, Kakiuchi F, Konster RG, Larrow JF, Tokunga M (1997) *Tetrahedron Lett* 38:773
- Wu MH, Jacobsen EN (1998) *J Org Chem* 63:5252
- Wu MH, Hansen KB, Jacobsen EN (1999) *Angew Chem Int Ed* 38:2012
- Gigante B, Corma A, Garcia H, Sabata MJ (2000) *Catal Lett* 68:113
- Angelino MD, Labinis PE (1999) *J Polym Sci A Polym Chem* 37:3888
- Jacobsen EN (2000) *Acc Chem Res* 33:421
- Paddock RL, Nguyen ST (2001) *J Am Chem Soc* 123:11498
- Shen Y-M, Duan W-L, Shi M (2003) *J Org Chem* 68:1559
- Solomon EI, Brunold TC, Davis MI, Kemsley JW, Lee SK, Lehnert N, Neese F, Skulan AJ, Yang YS, Zhou J (2000) *Chem Rev* 100:235
- Ohlendorf DH, Lipscomb JD, Weber PC (1988) *Nature* 336:403
- Ohlendorf DH, Orville AM, Lipscomb JD (1994) *J Mol Biol* 244:586
- Sivasubramanian VK, Ganesan M, Rajagopal S, Ramaraj R (2002) *J Org Chem* 67:1506
- Sivasubramanian VK, Ganesan M, Rajagopal S, Ramaraj R (unpublished work)
- Li F, Meier KK, Cranswick MA, Chakrabarti M, Van Heuvelen KM, Munck E, Que L Jr (2011) *J Am Chem Soc* 133:7256
- Premsingh S, Venkataramanan NS, Rajagopal S, Mirza SP, Vairamani M, Rao PS, Velavan K (2004) *Inorg Chem* 43:5744
- Collman PJ, Zeng L, Brauman I (2004) *Inorg Chem* 43:2672
- Groos Z, Ini S (1997) *J Org Chem* 62:5514
- Palucki M, Finney NS, Pospisil PJ, Guler ML, Ishida T, Jacobsen N (1998) *J Am Chem Soc* 120:948
- Mansuy D (1993) *Coord Chem Rev* 125:129
- Li H, Lee LS, Schulze DG, Guest CA (2003) *Environ Sci Technol* 37:2686

60. Goto Y, Watanabe Y, Fukuzumi S, Jones JP, Dinnocenzo JP (1998) *J Am Chem Soc* 120:10762
61. Goto Y, Matsui T, Ozaki S, Watanabi Y, Fukuzumi S (1999) *J Am Chem Soc* 121:9497
62. Goodin DB, Me Ree DE (1993) *Biochemistry* 32:3313
63. Battioni P, Renaud JP, Bartoli JF, Reina-Artiles M, Fort M, Mansuy D (1988) *J Am Chem Soc* 110:8462
64. Anelli PL, Banfi S, Montanari F, Quici S (1989) *Chem Commun* (12):779
65. Bahramian B, Mirkhani V, Tangestaninejad S, Moghadam M (2006) *J Mol Cat A* 244:139
66. Gerloch M, Lewis J, Mabbs FE, Richards A (1968) *J Chem Soc A* 112
67. Gulloti M, Casella L, Pasini A, Ugo R (1977) *J Chem Soc Dalton Trans* (4):339
68. Gerloch M, Mabbs FE (1967) *J Chem Soc A* 1598
69. Hobday MD, Smith TD (1973) *Coord Chem Rev* 9:311
70. Karunakaran C, Kamalam M (2002) *J Org Chem* 67:1118